Original Research

Encoding Strategies for Three-Direction Phase-Contrast MR Imaging of Flow[1]

Norbert J. Pelc, ScD • Matt A. Bernstein, PhD
Ann Shimakawa, MS • Gary H. Glover, PhD

Three encoding strategies for the measurement of flow velocities in arbitrary directions with phase-contrast magnetic resonance imaging are presented; their noise and dynamic range performance are compared by means of theoretical analysis and computer simulation. A six-point measurement strategy is shown to be quite inefficient in terms of velocity variance per unit time. A simple four-point method exhibits equal dynamic range; its noise depends on flow direction but on average is equal to that of the six-point method. An alternate, balanced four-point method has noise that is direction independent and has, depending on implementation, possibly lower noise levels. Either four-point method is more efficient and is preferred over the six-point approach.

Index terms: Flow imaging • Image processing • Model, mathematical • Phase-contrast imaging • Physics • Three-dimensional imaging

JMRI 1991; 1:405–413

SPURRED BY CONSTANT IMPROVEMENTS over several years, vascular magnetic resonance (MR) imaging has progressed to the point that a clinical role for this technique is nearly assured. Among the methods that have been used for vascular MR imaging are time of flight (1), inflow enhancement (2), and phase-contrast techniques (3).

The phase-contrast MR methods are based on the fact that the transverse magnetization of spins that move in the presence of a magnetic field gradient obtain a different phase than static spins (4). Specifically, if constant velocity motion is assumed and no refocusing radio-frequency pulses are used, the phase shift at time T after the transverse magnetization is created is proportional to the product of velocity and the first moment of the gradient waveform:

$$\phi(T) = \gamma v \int_0^T G(t)\, t\, dt. \qquad (1)$$

Early efforts toward imaging motion or flow attempted to obtain this information from a single imaging experiment and assumed that the phase in the resulting image was due only to motion in the direction of interest (5,6). Unfortunately, image phase can also be affected by many other phenomena, including pulse sequence timing, B_0 inhomogeneity, radio-frequency effects, magnetic field eddy currents, and motion in other directions. More reliable methods use multiple measurements and rely not on the absolute phase but on phase shifts observed as the magnetic field gradient waveforms are altered (7–12).

The simplest of these phase-contrast methods, referred to here as the "two-point method," uses two measurements, each made with a different magnetic field gradient waveform along one direction to examine motion in that direction (10,11). Motion in all directions has been studied with a "six-point method" that uses three pairs of measurements, each pair sampling the motion along one Cartesian direction (3).

The purpose of this report is to examine several alternatives for the encoding and processing of phase-contrast MR data. In particular, two four-point meth-

[1] From the Department of Diagnostic Radiology and Nuclear Medicine, S-047, Stanford University School of Medicine, 300 Pasteur Dr, Stanford, CA 94305-5105 (N.J.P., G.H.G.); and GE Medical Systems, Waukesha, Wis (M.A.B., A.S.). Received January 22, 1991; revision requested March 26; revision received April 15; accepted April 24. **Address reprint requests to** N.J.P.

See also the articles by Dumoulin et al (pp 399–404) and Hausmann et al (pp 415–422) in this issue.

ods capable of measuring motion in arbitrary directions are presented and shown to be more time efficient than the six-point method. A previous analysis of noise in phase images (13) is extended to describe the noise performance of these encoding strategies. The characteristics of these methods are derived and compared by means of computer simulations.

• THEORY

Signal-to-Noise Ratio and Processing Strategies in Two-Point Methods

Throughout this article, the terms "point" and "measurement" correspond to the acquisition of sufficient data for an entire image. In two-dimensional Fourier transform imaging, for example, this includes acquisitions with all phase-encoding gradient amplitudes but with a constant first moment. A caret indicates an estimate. For example, $\hat{v}$ is an estimate of the true velocity v. The value of $\hat{v}$ may differ from v because of noise or deterministic errors. Except where noted, each voxel is assumed to have a single, well-defined velocity vector and all spins in the voxel are assumed to move similarly. Nonuniform flow velocity within a voxel is more difficult to analyze, but as long as the nonuniformity is small (relatively uniform phase shifts and relatively constant signal magnitude as a function of gradient moment), the flow within the voxel can be treated as having a uniform effective velocity, where the effective velocity is that which would produce the measured net phase shift. The effect of nonconstant velocity (eg, pulsatile motion) is not considered here. However, the analysis is relevant to a single frame in a gated study if the motion is periodic and higher-order motion effects are small. Further, the complications due to nonconstant motion do not affect the major purpose of the present analysis: the comparison of the encoding strategies.

Suppose a voxel contains both static and moving spins, but assume that the moving spins all have the same velocity v. With the two-point method, two measurements are made, yielding signals S_1 and S_2. The contributions to S_1 from static and moving spins are S_s and S_m, respectively. Because of field inhomogeneities and the effects of motion, S_s and S_m are complex quantities with possibly different phase. S_2 is measured with the first moment of the gradient in the direction of v altered by ΔM_1, thereby causing the phase of the signal from moving spins to shift by $\phi_m = \gamma \Delta M_1 v$. The two measurements are

$$\begin{aligned} S_1 &= S_s + S_m, \\ S_2 &= S_s + S_m e^{i\phi_m}. \end{aligned} \tag{2}$$

Two methods of processing these data have been reported. In one (3), the complex difference of the two measurements is computed, yielding

$$\begin{aligned} \Delta S &= S_m (e^{i\phi_m} - 1) \\ &= 2\, i\, S_m \sin \frac{\phi_m}{2}. \end{aligned} \tag{3}$$

The magnitude of the complex-difference image is computed to avoid problems due to spatial variations in the phase of S_m. The final image signal then is

$$|\Delta S| = 2\,|S_m \sin \frac{\phi_m}{2}|. \tag{4}$$

This method has several advantages; among them is its simplicity, as it requires minimal modification to the imager software. The difference can be computed before image reconstruction, therefore requiring less data storage. Also, $|\Delta S|$ is approximately zero whenever there is no motion ($\phi_m = 0$) or in regions of low flow signal intensity (eg, outside the object, $S_m \approx 0$). Finally, the output is independent of any static signal S_s that might be present. The principal disadvantage of this approach is that the magnitude operation discards the direction information contained in the sign of ϕ_m. Also, if the difference is computed prior to the Fourier transform (to reduce memory requirements), information about static structures is lost.

An alternative phase-difference approach has also been reported (10–12). Here, separate reconstructions must be performed on each data set and the phase difference at each point is computed:

$$\begin{aligned} \Delta\phi &= \arg S_2 - \arg S_1 \\ &= \arg S_2/S_1, \end{aligned} \tag{5}$$

where arg C indicates the phase of the complex signal C. An apparent velocity image $\hat{v}$ is then formed:

$$\hat{v} = \frac{\Delta\phi}{\gamma \Delta M_1}. \tag{6}$$

The main advantages of this method are that direction information is retained and, in some cases, velocities and flow can be quantitated. For example, if the voxel has no static signal, $\Delta\phi$ equals ϕ_m and $\hat{v}$ equals v. In general, however, the measured phase shift depends on S_s and $\Delta\phi$ underestimates ϕ_m. Another advantage of this phase-difference approach is that, since two complete complex images are produced, a magnitude image that portrays static structures is easily obtained, for example as $|S_1|$, $|S_2|$, or $(|S_1| + |S_2|)/2$. Of course, if its memory requirements are increased, the complex-difference method can also produce static signal images, for example by retaining the original data sets.

One aesthetic disadvantage of the phase-difference approach is that the noise depends strongly on signal strength. If the in-phase and quadrature components are assumed to have equal and uncorrelated noise in each complex image, with variance σ^2, the variance in each phase image can be shown to be (13)

$$\sigma_\phi^2 = \frac{\sigma^2}{|S|^2}, \tag{7}$$

where $|S|$ is the magnitude of the signal in the voxel of interest. If both measurements have comparable signal magnitude ($|S_1| \approx |S_2| \approx |S|$), the variance in the measured phase difference is twice σ_ϕ^2. Combining this

with Equation (6), we obtain the variance in the velocity image:

$$\sigma_v^2 = \frac{2\sigma^2}{|\gamma \Delta M_1 S|^2}. \quad (8)$$

The dependence of σ_v^2 on the signal level $|S|$ is particularly disturbing in regions of no signal (eg, outside the object or in air-filled cavities), where the measured phase difference is arbitrary. This aesthetic problem can be alleviated by setting the velocity image to zero in all voxels in which signal magnitude is below some threshold. Disadvantages of this thresholding are the somewhat arbitrary choice of threshold and that the image noise level remains dependent on signal magnitude. One operation that mitigates these problems is the formation of an image in which the pixel intensities are equal to the product of the velocity image and the signal magnitude (magnitude-weighted velocity image):

$$F = |S|\hat{v}. \quad (9)$$

Such images have some interesting properties. The images do not have extremely high noise level in regions of low signal intensity. In contrast to the complex-difference method, the direction information present as the sign of $\hat{v}$ is retained. Quantification is still possible because the scaling applied to the image is known. Finally, the appearance of moving structures is relatively independent of overlapped static signal, since S_s will generally cause the apparent velocity $\hat{v}$ to decrease but the signal magnitude $|S|$ to increase.

Six-Point Method

The six-point method uses three pairs of points to measure the three Cartesian velocity components $\hat{v}_x$, $\hat{v}_y$, and $\hat{v}_z$. The three components can be added in quadrature to compute the speed:

$$\hat{v}_6 = \sqrt{\hat{v}_x^2 + \hat{v}_y^2 + \hat{v}_z^2}. \quad (10)$$

Assuming that the same number of averages, and so forth, are used for each component as in the two-point method, imaging time is tripled. Further, if the same first-moment change ΔM_1 is used for each direction, each velocity component has independent noise, with variance given by Equation (8). The variance in the speed can be computed from the variance in each component (14). Since, for example, $\partial \hat{v}_6 / \partial \hat{v}_x = \hat{v}_x / \hat{v}_6$, the variance in $\hat{v}_6$ is

$$\sigma_6^2 = \frac{2\sigma^2}{|\gamma \Delta M_1 S|^2}. \quad (11)$$

It can be seen that a large penalty results from lack of knowledge of the direction of motion. If the direction is known and used to measure the motion with two points, the variance in the measured velocity is given by Equation (8). If, on the other hand, the direction is not known and the six-point method is used, imaging time is tripled but the variance is unchanged.

Simple Four-Point Method

The two-point method can be interpreted as consisting of one measurement that provides a phase reference and another that is differentially encoded. When viewed this way, the six-point method uses an independent phase reference for each direction. If, instead, a single phase reference is used, only four points are needed, one providing a phase reference ϕ_0 and one differentially encoded in each direction, providing ϕ_x, ϕ_y, and ϕ_z. The velocity components are then computed by subtracting ϕ_0 from ϕ_x, ϕ_y, and ϕ_z:

$$\hat{v}_x = \frac{\phi_x - \phi_0}{\gamma \Delta M_1},$$

$$\hat{v}_y = \frac{\phi_y - \phi_0}{\gamma \Delta M_1}, \quad (12)$$

$$\hat{v}_z = \frac{\phi_z - \phi_0}{\gamma \Delta M_1}.$$

The speed is calculated as in the six-point method:

$$\hat{v}_4 = \sqrt{\hat{v}_x^2 + \hat{v}_y^2 + \hat{v}_z^2}. \quad (13)$$

As before, the variance in each velocity component is given by Equation (8). However, unlike in the six-point method, the errors in the velocity components are correlated because of their use of a common reference. The covariance between $\hat{v}_x$ and $\hat{v}_y$ is

$$\sigma_{xy}^2 = \frac{\sigma^2}{|\gamma \Delta M_1 S|^2}. \quad (14)$$

There is a similar covariance between the other velocity pairs. These variances and covariances can be used to compute the variance in $\hat{v}_4$ (14):

$$\sigma_4^2 = \frac{\sigma^2}{|\gamma \Delta M_1 S|^2}\left[1 + \frac{(v_x + v_y + v_z)^2}{v^2}\right], \quad (15)$$

where v is the speed.

The noise in the speed estimate is direction dependent. For motion in a Cartesian direction, the term in brackets equals 2 and the noise is equal to that in the six-point method. When v_x and v_y have the same sign, the contributions to σ_4^2 of the noise in the ϕ_0 measurement through the v_x and v_y terms add, whereas these contributions cancel when v_x and v_y have opposite signs. In the worst case, the three Cartesian components are equal, the term in brackets equals 4, and the variance is twice that of the six-point method. In some directions, however, the noise correlation reduces the term in brackets. In the best case, it equals 1 and the variance is half that of the six-point method. An interesting parameter for characterizing the simple four-point method is its performance averaged over all directions. In a polar coordinate system with speed v and polar and azimuthal angles α and β, respectively, $v_x = v \cdot \sin\alpha \cdot \cos\beta$, $v_y = v \cdot \sin\alpha \cdot \sin\beta$, and

$v_z = v \cdot \cos \alpha$. Averaging over a sphere of radius V, the average variance is

$$\overline{\sigma_4^2} = \frac{1}{\frac{4}{3}\pi V^3} \int_0^V v^2 \, dv \int_0^\pi \sin \alpha \, d\alpha \int_0^{2\pi} \sigma_4^2 \, d\beta$$

$$= \frac{\sigma^2}{|\gamma \Delta M_1 S|^2} \left\{ 1 + \frac{1}{4\pi} \int_0^\pi \sin \alpha \, d\alpha \cdot \int_0^{2\pi} [\cos \alpha + \sin \alpha (\cos \beta + \sin \beta)]^2 \, d\beta \right\}, \quad (16)$$

which yields

$$\overline{\sigma_4^2} = \frac{2\sigma^2}{|\gamma \Delta M_1 S|^2}. \quad (17)$$

Note that the average variance is independent of the radius of the averaging sphere and is equal to that of the six-point method.

Balanced Four-Point Method

In this method, the flow-encoding first moments are altered in pairs. As in the simple four-point method, the data acquired with the first sequence of the balanced four-point method can be interpreted as a phase reference. For the second sequence, the gradient first moments along two directions (eg, $\vec{x}$ and $\vec{y}$) are each altered by ΔM_1. The complex image data are represented by

$$S_2 = S_1 e^{i\phi_x} e^{i\phi_y}, \quad (18)$$

where we have assumed no static signal, S_1 represents the data from the first sequence, $\phi_x = \gamma \Delta M_1 v_x$, and $\phi_y = \gamma \Delta M_1 v_y$. For the third and fourth sequences, the moments along $\vec{x}$ and $\vec{z}$, and $\vec{y}$ and $\vec{z}$, respectively, are changed by ΔM_1 as compared with those of the first sequence. With $\phi_z = \gamma \Delta M_1 v_z$, the complex image data produced by these two sequences are represented by

$$\begin{aligned} S_3 &= S_1 e^{i\phi_x} e^{i\phi_z}, \\ S_4 &= S_1 e^{i\phi_y} e^{i\phi_z}. \end{aligned} \quad (19)$$

Although the desired result can be derived directly, it is perhaps helpful to notice that

$$\begin{aligned} \phi_2 - \phi_1 &= \phi_x + \phi_y, \\ \phi_3 - \phi_1 &= \phi_x + \phi_z, \\ \phi_4 - \phi_1 &= \phi_y + \phi_z, \end{aligned} \quad (20)$$

where $\phi_i = \arg(S_i)$, for i equal to 1 through 4. From Equation (20) and the known proportionality between the phase shifts and the velocity components, it can be shown that

$$\begin{aligned} \hat{v}_x &= \frac{-\phi_1 + \phi_2 + \phi_3 - \phi_4}{2\gamma \Delta M_1}, \\ \hat{v}_y &= \frac{-\phi_1 + \phi_2 - \phi_3 + \phi_4}{2\gamma \Delta M_1}, \\ \hat{v}_z &= \frac{-\phi_1 - \phi_2 + \phi_3 + \phi_4}{2\gamma \Delta M_1}. \end{aligned} \quad (21)$$

Table 1
Encoding/Decoding Matrix for the Balanced Four-Point Method

Measurement	Direction		
	x	y	z
1	−1	−1	−1
2	+1	+1	−1
3	+1	−1	+1
4	−1	+1	+1

Note.—The value −1 or +1 represents the low or high state, respectively, of the first moment in the relevant direction. For decoding, a +1 indicates that the phase value adds to the velocity estimate and a −1 indicates that it subtracts from the estimate.

Note that all measurements contribute to all velocity components. Table 1 shows another way to describe the encoding and decoding used in this method. The first measurement has all the moments in their lowest (most negative) state, the second has the $\vec{x}$ and $\vec{y}$ directed moments increased by ΔM_1, and so on. The same table entries are used in decoding the measured data. In the x column, we see that for computing $\hat{v}_x$ the phases of the second and third measurements are added to and the phases of the first and fourth are subtracted from the estimate. This process has some similarities with Hadamard encoding (15). Note also that for each velocity, two phase measurements are added and two are subtracted. Thus, any additive phase shifts common to the four measurements are canceled.

The variance in each velocity component is easily calculated from Equation (21). Since the phase measurements have equal and independent noise, with variance given by Equation (7), the velocity components have equal variance:

$$\sigma_{v_x}^2 = \sigma_{v_y}^2 = \sigma_{v_z}^2 = \frac{\sigma^2}{|\gamma \Delta M_1 S|^2}. \quad (22)$$

For the same ΔM_1, this method has half the variance of the two-point method. Imaging time has been doubled, but the entire imaging time increase is reflected in the improved precision. Thus, this four-point method is quite efficient. This result is intuitively acceptable by observation that each flow component is effectively measured twice in the four experiments. For example, $\hat{v}_x$ is measured by S_1 and S_2 as a pair, and independently again by S_3 and S_4 as a pair. What is perhaps more surprising is that the velocity components given by Equation (21) have independent noise, and when they are combined to compute the "balanced" speed $\hat{v}_b$,

$$\hat{v}_b = \sqrt{v_x^2 + v_y^2 + v_z^2}, \quad (23)$$

the resulting variance is

$$\sigma_b^2 = \frac{\sigma^2}{|\gamma \Delta M_1 S|^2}. \quad (24)$$

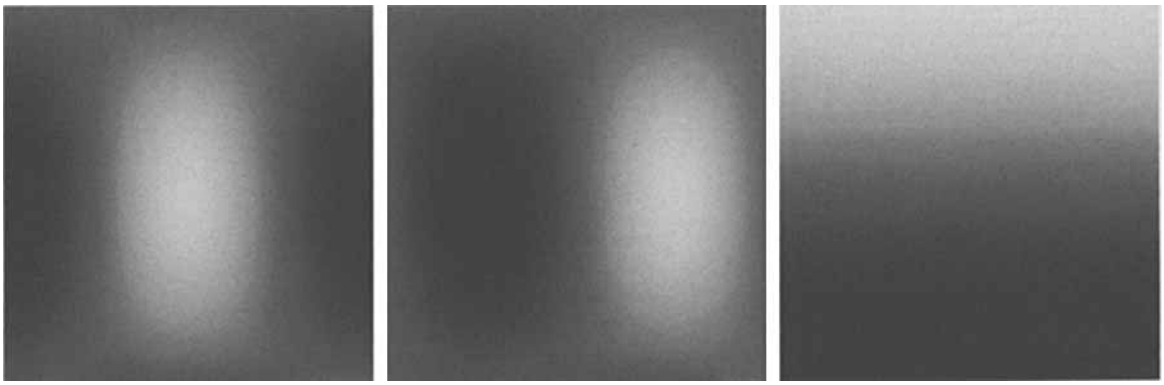

a. b. c.

Figure 1. The x- **(a)**, y-**(b)**, and z-directed **(c)** velocity components for the simulated object in which direction of motion varies spatially, imaged by the six-point method. All possible motion directions are included.

The efficiency of this method is retained even in the speed measurement (compare Eqq [24] and [8]). Further, the variance in the estimated speed is independent of direction, hence the term balanced.

Aliasing and Dynamic Range

With any of the measurement methods, the variance can be reduced by increasing ΔM_1. However, because only phase shifts in a 2π range can be uniquely measured, the range of velocities that can be measured is also limited. If there is no a priori knowledge of the velocity being measured, and assuming positive and negative velocities are equally likely, measured phase shifts lie between $-\pi$ and π; therefore, for example, an actual phase shift of $\pi + \epsilon$ will be incorrectly interpreted as $-\pi + \epsilon$ and lead to a velocity mismap. This phenomenon is exactly analogous to spatial aliasing (wraparound) in MR imaging and is termed velocity or flow aliasing. Since increasing ΔM_1 will decrease both the variance and the range of velocities that can be measured, any comparison of precision is potentially misleading unless the dynamic range of velocity is also considered. In examining dynamic range, we assume that no correction for aliasing is used.

Let v_{max} be the maximum speed that can be measured in a particular direction without aliasing, and define v_{enc} as

$$v_{enc} = \frac{\pi}{\gamma \Delta M_1}. \qquad (25)$$

For the six-point and simple four-point methods, the worst case (smallest v_{max}) is motion along any Cartesian direction, where $v_{max} = v_{enc}$. The best cases are those with equal absolute value components along each direction, where $v_{max} = \sqrt{3} v_{enc}$. The balanced four-point method exhibits aliasing when either $(\phi_2 - \phi_1)$, $(\phi_3 - \phi_1)$, or $(\phi_4 - \phi_1)$ are outside the $\pm\pi$ range. The worst cases are $(v_x = v_y, v_z = 0)$, $(v_x = v_z, v_y = 0)$, and $(v_y = v_z, v_x = 0)$, where $v_{max} = v_{enc}/\sqrt{2}$. Note that for the same ΔM_1, this method has a smaller worst-case dynamic range. The best cases for dynamic range with this method are $(v_x = v_y, v_z = -3v_x)$, $(v_x = v_z, v_y = -3v_x)$, and $(v_y = v_z, v_x = -3v_y)$, where $v_{max} = \sqrt{11/4} v_{enc}$. The details of the direction dependence of v_{max} are presented in more detail below.

If the value of ΔM_1 is limited by available gradient strength and time, the noise comparison presented above is relevant. In other cases, ΔM_1 may be selected for dynamic-range reasons. Because of the strong relationship between precision and dynamic range (through ΔM_1), comparison of the encoding strategies at a constant dynamic range is of interest. For example, suppose that it is necessary to ensure that all velocities with magnitude less than or equal to v_m be measured correctly regardless of direction. With the six-point or simple four-point method, we would choose $\Delta M_1 = \pi/(\gamma v_m)$. The balanced four-point method must use a smaller moment change, $\Delta M_{1,b} = \pi/(\sqrt{2}\gamma v_m)$. This factor of $\sqrt{2}$ will increase the variance (cf Eq [24]) by a factor of two. Thus, for constant minimum dynamic range, the variance with the balanced four-point method and the average variance with the simple four-point method (Eq [17]) are equal.

• COMPUTER SIMULATIONS

The noise and dynamic-range performance of the three encoding methods were tested by means of computer simulations.

Noise for the simulations was obtained by acquiring data with an MR imaging system (Signa; GE Medical Systems, Milwaukee) with the transmitter disabled, a 50-Ω load connected to the preamplifier, and a typical receiver gain setting. Fourier transformation was performed, and complex images were retained. All further simulation was performed in image space. To efficiently demonstrate the relative performance of the techniques and direction dependence of noise, a planar object with motion in all directions was simulated. The object had constant-speed motion at all locations, but motion direction depended on location in the plane. Let v be the speed and describe the motion in polar coordinates as $v_z = v \cdot \cos\alpha$, $v_x = v \cdot \sin\alpha \cdot \cos\beta$, and $v_y = v \cdot \sin\alpha \cdot \sin\beta$. In the simulated object, α varied from 0 to π from top to bottom, while β varied from $-\pi$ to π from left to right (Fig 1). Thus, at the top and bottom of this plane, the motion was in the posi-

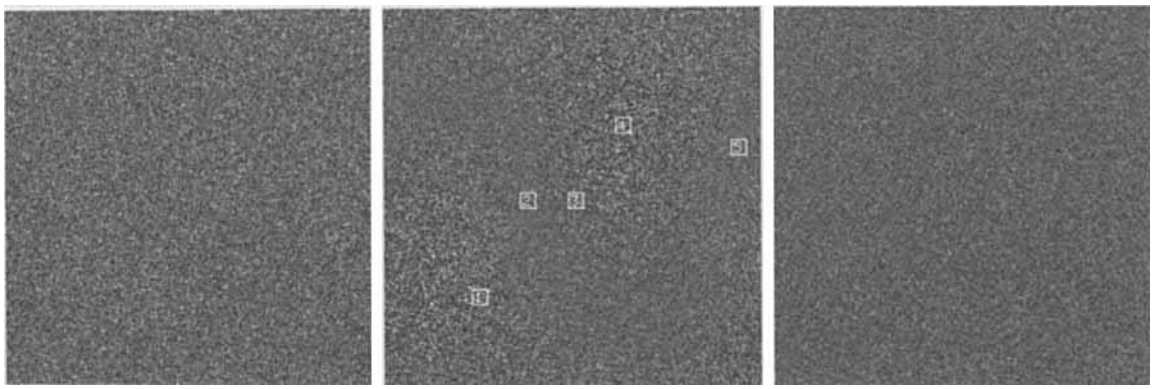

a. **b.** **c.**

Figure 2. Speed images generated by each of the three methods: six-point **(a)**, simple four-point **(b)**, and balanced four-point **(c)**, assuming equal ΔM_1. Direction dependence of noise with the simple four-point method can be seen in **b.** Regions shown in **b** were analyzed quantitatively (Table 2). The balanced four-point method **(c)** has a uniform and lower noise level.

tive and negative z directions, respectively, while in the central horizontal line the motion direction was in the x-y plane, with motion in the center of the image being in the positive x direction. This arrangement of motion directions was discretized to 256 values in α and β. The value of $\gamma\Delta M_1$ was arbitrarily set to unity, and the simulated speed was set so that $\gamma\Delta M_1 v = \pi/2$. The image-space signal was assumed to be constant throughout the plane, real when all first moments were in their low states, and such that the image signal-to-noise ratio (S/σ) of each measurement was equal to 10. For each point in the object and for the three encoding strategies, the appropriate values of α and β were used to compute the velocity components. The expected phase shifts for each measurement were calculated and converted to complex image signals. Noise was added to these, and the simulated signals were then decoded to compute images of velocity components and speed. For display purposes, these computed images were scaled by a factor of 1,000. Region-of-interest noise measurements were performed in selected areas.

Aliasing with the simple and balanced four-point methods was studied. The six-point method was not treated because its behavior is identical to that of the simple four-point method. The distribution of motion direction described above was used to demonstrate the direction dependence of dynamic range. At each point in a 256 × 256 array, the appropriate values of α and β were used to compute the relative velocity components. For the simple and balanced four-point methods, these were converted into relative phase shifts, and the motion speed (v_{max}) that would cause the largest absolute-value phase shift to equal π was calculated. Thus, for the simple four-point method,

$$v_{max,\,4\,pt} \propto \frac{1}{\max\left(\left|\frac{v_x}{v}\right|, \left|\frac{v_y}{v}\right|, \left|\frac{v_z}{v}\right|\right)}, \qquad (26)$$

where $v = \sqrt{v_x^2 + v_y^2 + v_z^2}$. Similarly, for the balanced four-point method,

$$v_{max,\,bal} \propto \frac{1}{\max\left(\left|\frac{v_x + v_y}{v}\right|, \left|\frac{v_x + v_z}{v}\right|, \left|\frac{v_y + v_z}{v}\right|\right)}. \qquad (27)$$

For each method, images proportional to v_{max} were generated.

Aliasing was also studied by simulation of an object spinning about the z axis and imaged axially. As seen on the image, rotation was in the counterclockwise direction. The values of v_x and v_y were proportional to position in the vertical and horizontal directions, respectively, while v_z was 0. To allow aliasing to be viewed, the rotation rate and ΔM_1 were selected so that at the horizontal extreme of the image, $\gamma\Delta M_1 v_y = 2\pi$. As before, the image signal with all moments in their low state was assumed to be real. For both four-point methods and for each location in the object, the local velocity was used to compute the expected signals. All computed phase values were constrained to be between $-\pi$ and π by adding or subtracting multiples of 2π. Assuming that the first measurement produces a real signal yields no loss of generality, and the results are analogous to constraining all measured phase shifts relative to the first measurement to be in the $\pm\pi$ range. Images of the apparent velocity components were generated.

• RESULTS

Figure 1 shows the three velocity components from the simulation of the object with position-dependent motion direction, as measured with the six-point method. These aid in the appreciation of motion direction throughout the object. The images with the other two techniques were identical except for noise. Figure 2 shows the speed images produced by the three strategies. As expected, noise is uniform with the six-point method (Fig 2a) and the balanced four-point method (Fig 2c). The standard deviation measured over each entire image is 14.12 and 10.06, respectively, in excellent agreement with theoretical predictions of 14.14 and 10 (Eqq [11], [24]). The direction dependence of noise with the simple four-point method is evident visually in Figure 2b. The

Table 2
Relative Velocity Components and Direction-dependent Noise with the Simple Four-Point Method

Region	$\frac{v_x}{v}$	$\frac{v_y}{v}$	$\frac{v_z}{v}$	Noise	
				Expected	Measured
1	0	$-\frac{1}{\sqrt{2}}$	$-\frac{1}{\sqrt{2}}$	17.32	17.8 ± 1.4
2	$\frac{1}{\sqrt{2}}$	$-\frac{1}{\sqrt{2}}$	0	10.00	9.9 ± 0.8
3	1	0	0	14.14	14.2 ± 1.1
4	$\frac{1}{\sqrt{3}}$	$\frac{1}{\sqrt{3}}$	$\frac{1}{\sqrt{3}}$	20.00	21.8 ± 1.7
5	$-\frac{2}{\sqrt{6}}$	$\frac{1}{\sqrt{6}}$	$\frac{1}{\sqrt{6}}$	10.00	9.4 ± 0.7

Note.—Measured and expected noise for the regions shown in Figure 2b. Measured values are the standard deviation in each region ± one standard deviation in the measurement, the latter estimated as $\sigma/\sqrt{2(N-1)}$, where N is the number of pixels used (N=81) (14).

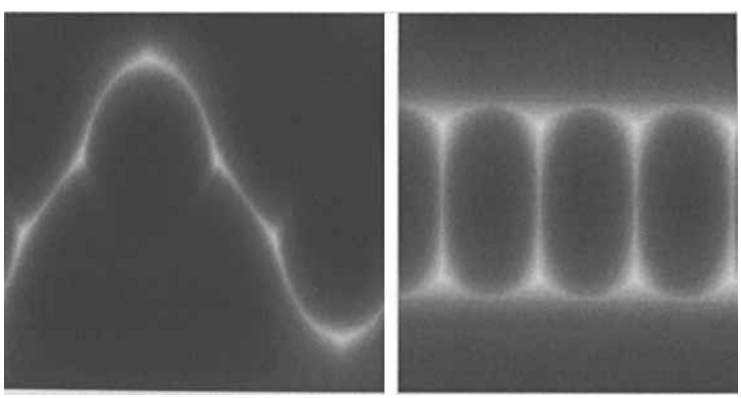

a. b.

Figure 3. Direction dependence of dynamic range with the simple four-point **(a)** and balanced four-point **(b)** methods, assuming equal ΔM_1. Local brightness is proportional to v_{max} in the corresponding direction. The minimum dynamic range (darkest area) is smaller with the balanced method.

noise levels measured in each of the five regions shown on Figure 2b are listed in Table 2 and compare well with theoretical predictions (Eq [15]).

Figure 3 shows the direction dependence of dynamic range with the simple and balanced four-point methods. In these images, local brightness is proportional to v_{max} in the corresponding direction. Note, for example, that in Figure 3a the dynamic range minima (dark regions) occur when motion is in a Cartesian direction, while maxima (bright regions) occur when all velocity components are equal. Similarly, in Figure 3b the dynamic-range maxima occur when phase shifts due to multiple velocity components cancel (cf Eq [27]). Region-of-interest measurements on these images agree with theoretical predictions (Eqq [26], [27]). Figure 4a–c shows the images of the simulation of the spinning object obtained with the simple four-point method. The sudden dark/bright transitions are at the locations where v_x and/or v_y produce phase shifts of $\pm\pi$. The region of velocities that are correctly measured is the central square. Figure 4d–e shows the analogous result with the balanced four-point method. The central hexagonal region contains the velocities that are well measured and reflects the smaller minimum dynamic range achieved with this method as opposed to the simple four-point method when the same ΔM_1 is used. Note that, in contrast to the simple four-point method, when the balanced method aliases, all velocity components may be in error. For example, even though v_z is zero, there are regions where there is an apparent nonzero velocity in this direction due to aliasing of some of the phase-shift measurements.

• DISCUSSION

Of the two processing strategies, complex difference versus phase difference, the phase-difference method is preferred because of its retention of direction information, potential for quantitative use, and ability to display static structures. Incorporation of magnitude weighting into the phase-difference technique obviates the aesthetic difficulties in regions of low signal intensity. Also, the complex-difference method is not compatible with balanced four-point encoding. However, the signal-to-noise comparison presented here is relatively independent of these processing choices.

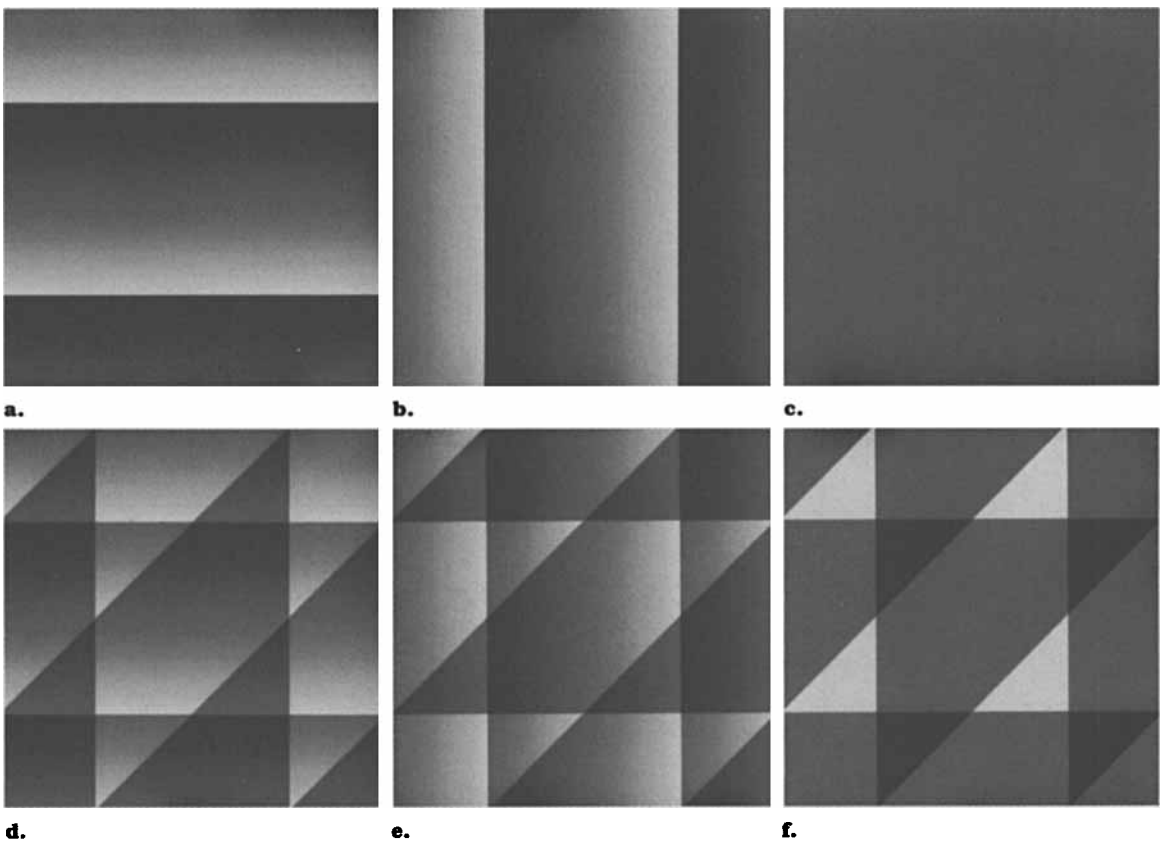

Figure 4. Computer simulation of a spinning object to demonstrate aliasing. Shown are the x- **(a)**, y- **(b)**, and z-directed **(c)** velocities as imaged by the simple four-point method. Aliasing along each direction is independent. The analogous results with the balanced method **(d–f)** demonstrate a smaller minimum dynamic range (minimum distance of aliased points to the image center) and coupled aliasing (note aliasing in **f**, even though the velocity in the z direction is zero).

All three techniques for the measurement of arbitrarily directed velocity are completely immune to "static" position-dependent phase shifts, and only the local change in phase resulting from a change in the first moment is used to measure velocity. This is particularly necessary if gradient-echo images are used to measure blood flow velocity because these images can exhibit very large local phase shifts due to magnetic field inhomogeneity and/or chemical shift. The absolute first moments used are not critical. One may choose to operate with first moments near zero so as to minimize intravoxel dephasing, but the critical parameter for the present methods is the change applied to the first moment.

Table 3 summarizes the relative advantages and disadvantages of the four encoding strategies. The six-point method triples the minimum imaging time compared with the two-point method, in which it is assumed that motion direction is known. Unfortunately, this imaging time increase is unaccompanied by an improvement in the precision of the velocity estimate.

The simple four-point method has exactly the same dynamic range as the six-point method. Use of a common phase reference causes the noise in the measured velocity components to be correlated and the noise in the measured speed to be direction dependent. The variance in the speed ranges over a factor of four but on average is the same as that in the six-point and two-point methods. If we define efficiency as variance per unit time and assign the two-point method an efficiency of 1, the six-point method has an efficiency of ⅓ and the average efficiency of the simple four-point method is ½.

The imperfect efficiency in speed measurements with the latter two methods can be understood by considering motion along a Cartesian direction. With the six-point method, two-thirds of the imaging time is dedicated to the measurement of velocity components that do not contribute to the speed estimate or its variance. Thus, all this time is wasted. With the simple four-point method, this time waste is reduced to one-half of the imaging time.

The balanced four-point method was developed with the aim of eliminating the direction dependence of the simple four-point method and improving its efficiency. All measurements contribute equally to the variance of each velocity component, and in a manner reminiscent of Hadamard encoding, the noise in each component is independent of the noise in the others. As a result, the noise in the measured speed is direction independent. If the balanced method uses the same first-moment changes along each Cartesian direction as the other methods, the variance in the measured speed is half that of the six-point method.

Table 3
Relative Performance Summary of Encoding Methods

Method	Imaging Time	Variance	Minimum Dynamic Range	Efficiency: Constant ΔM_1	Efficiency: Constant Dynamic Range	Comments
Two-point	1	1	1	1	1	Known direction
Six-point	3	1	1	⅓	⅓	· · ·
Simple four-point	2	1	1	½	½	Direction-dependent noise
Balanced four-point	2	½	$1/\sqrt{2}$	1	½	Coupled aliasing

Note.—All parameter values are relative to those of the two-point method.

The dynamic range of velocities that can be measured and the precision of the measurements are coupled because they are both determined by the first-moment changes that are used. The dynamic range can be described by the maximum velocity that can be measured without aliasing. For all the methods, v_{max} is direction dependent. If a single dynamic-range parameter is needed, the most rational choice is the minimum v_{max} along any direction. For constant first-moment change, the minimum v_{max} with the balanced four-point method is smaller by a factor of $\sqrt{2}$ than that with the other techniques. Also, with the balanced method, aliasing errors can appear in velocity components that are well within the range; with the other methods, aliasing is independent along each direction.

The balanced four-point method makes measurements encoded along $\vec{x} + \vec{y}$, $\vec{x} + \vec{z}$, and $\vec{y} + \vec{z}$. The vector summation of the first-moment changes is responsible for the $\sqrt{2}$ reduction in minimum v_{max}. The $\sqrt{2}$ increase in the instantaneous first-moment change can also be viewed as causing the reduction in noise. However, this method is not merely a coordinate rotation of the simple four-point method (ie, the encoded directions are not mutually orthogonal). Were it so, the noise would remain direction dependent.

Because of its different aliasing behavior, it is difficult to define a relative efficiency for the balanced method. With constant ΔM_1, the efficiency is 1, twice that of the simple four-point method and equal to that of the two-point method, but the minimum dynamic range is smaller. For constant minimum dynamic range, the efficiencies of this and the simple four-point method are equal. Thus, the relative advantage of the balanced method over the simple four-point method depends on the context in which it is used. If the first-moment changes along each gradient axis are limited by, for example, gradient strength and/or available time, the balanced method offers improved efficiency. If both methods are allowed to be optimized and limited only by minimum dynamic range, their average noise performance will be equal and the balanced method offers only its direction independence. ●

Acknowledgments: The authors thank Donna Cronister, BS, for help in the preparation of this manuscript, Charles Dumoulin, PhD, for encouragement and support, and Dwight Nishimura, PhD, for many helpful discussions on this subject.

References

1. Nishimura DG, Macovski A, Pauly JM, Conolly SM. MR angiography by selective inversion recovery. Magn Reson Med 1987; 4:193–202.
2. Ruggieri PM, Laub GA, Masaryk TJ, Modic MT. Intracranial circulation: pulse-sequence considerations in three-dimensional (volume) MR angiography. Radiology 1989; 171:785–791.
3. Dumoulin CL, Souza SP, Walker MF, Wagle W. Three-dimensional phase contrast angiography. Magn Reson Med 1989; 9:139–149.
4. Hahn EL. Detection of sea-water motion by nuclear precession. J Geophys Res 1960; 65:776–777.
5. van Dijk P. Direct cardiac NMR imaging of heart wall and blood flow velocity. J Comput Assist Tomogr 1984; 8:429–436.
6. Bryant DJ, Payne JA, Firmin DN, Longmore DB. Measurement of flow with NMR imaging using a gradient pulse and phase difference technique. J Comput Assist Tomogr 1984; 8:588–593.
7. Grover T, Singer JR. NMR spin-echo flow measurements. J Appl Phys 1971; 42:938–940.
8. Moran PR. A flow velocity zeugmatographic interlace for NMR imaging in humans. Magn Reson Imaging 1982; 1:197–203.
9. Feinberg DA, Crooks LE, Sheldon P, Hoenninger J, Watts J, Mitsuaki A. Magnetic resonance imaging of velocity vector components of fluid flow. Magn Reson Med 1985; 2:555–566.
10. O'Donnell M. NMR blood flow imaging using multiecho, phase contrast sequences. Med Phys 1985; 12:59–64.
11. Nayler GL, Firmin DN, Longmore DB. Blood flow imaging by cine magnetic resonance. J Comput Assist Tomogr 1986; 10:715–722.
12. Spritzer CE, Pelc NJ, Lee JN, Evans AJ, Sostman HD, Riederer SJ. Rapid MR imaging of blood flow with a phase-sensitive, limited-flip-angle, gradient recalled pulse sequence: preliminary experience. Radiology 1990; 176: 255–262.
13. Conturo TE, Smith GD. Signal-to-noise in phase angle reconstruction: dynamic range extension using phase reference offsets. Magn Reson Med 1990; 15:420–437.
14. Armitage P. Statistical methods in medical research. Oxford, England: Blackwell Scientific, 1971; 90–98.
15. Souza SP, Szumowski J, Dumoulin CL, Plewes DP, Glover GH. SIMA: simultaneous multislice acquisition of MR images by Hadamard-encoded excitation. J Comput Assist Tomogr 1988; 12:1026–1030.